

Evolution of Ordered Block Copolymer Serpentes into a Macroscopic, Hierarchically Ordered Web**

Suck Won Hong, Jun Wang, and Zhiqun Lin*

In the process of drying, a sessile drop containing nonvolatile solutes such as polymers, nanocrystals, and carbon nanotubes readily self-assembles into a number of concentric “coffee rings” through the repetitive “stick–slip” motion of a three-phase contact line.^[1] However, owing possibly to convection and a lack of control over the evaporation process of the drop, the rings are often irregular and stochastically organized.^[2] The challenge therefore remains to use evaporative self-assembly rationally to prepare such rings and other dissipative structures (e.g., fingering patterns^[3] and polygonal network structures^[4,5]) of high regularity and fidelity for use in microelectronics, data storage devices, and biotechnology applications. To date, only a few studies have focused on precise control of the evaporation process to produce such highly ordered structures.^[6–12] Surface patterning by controlled solvent evaporation offers a lithography- and external-field-free means to organize nonvolatile materials into ordered microscopic structures over large surface areas in a simple and cost-effective manner.

Control over the spatial arrangement of components (i.e., formation of hierarchically ordered structures) is highly desirable for many applications. To date, numerous studies have focused on creating hierarchically ordered structures using lithographic techniques. However, lithographic methods involve high processing and maintenance costs and require an iterative, multistep procedure that makes the structure formation process more complex and less reliable. Herein, we demonstrate a robust method to create hierarchically ordered structures consisting of diblock copolymers using two consecutive self-assembly processes at different length scales. First, the controlled evaporative self-assembly of a diblock copolymer solution, together with formation of fingering instabilities arising from the unfavorable interfacial interaction between one block and the substrate, occurs in a restricted geometry comprising a spherical lens on a flat substrate that yields concentric serpentes of diblock copolymer at the microscopic scale. Subsequently, upon solvent vapor annealing, these serpentes self-organize into a macroscopic web; at the same time, nanoscopic constituents of the

diblock copolymer self-assemble into domains oriented vertically to the web surface. The resulting highly ordered structures exhibit two independent characteristic dimensions: global web-like macrostructures with local regular microporous mesh arrays by a top-down mechanism; and, by a bottom-up approach, vertical nanoscopic domains of self-assembled diblock copolymer that span the entire web. In short, hierarchical structures are formed with significant potential for applications in optical and optoelectronic materials and devices.

Diblock copolymers composed of two chemically distinct chains covalently linked at one end are thermodynamically driven to self-assemble into a range of well-ordered nanoscopic domains (or nanodomains, historically called microdomains), for example, spheres, cylinders, and lamellae, depending on the volume fractions of their components.^[13–18] The size of the domains is dictated by the molecular weight of the polymer, typically in a range of 10 to 100 nm, which renders a density of 10^{13} nanostructures per square inch, an attractive alternative to fabricating nanometer-scale structures.

Thus, an asymmetric diblock copolymer, polystyrene-*b*-poly(methyl methacrylate) (PS-*b*-PMMA) with a cylindrical morphology was used as a nonvolatile solute and dissolved in toluene. The hydrophobic PS block forms nanocylinders within the hydrophobic PMMA matrix in PS-*b*-PMMA. A drop of PS-*b*-PMMA toluene solution was loaded in a restricted geometry composed of a spherical lens on a silicon substrate (i.e., “sphere-on-Si”, schematically illustrated in Figure 1 a), leading to a capillary-held polymer solution, the evaporation rate of which is highest at its extremity (see the Experimental Section).

In marked contrast to the copious past work in which a sessile drop was allowed to evaporate over the entire surface,^[1,2] evaporation in the sphere-on-Si geometry was restricted to the edge of the drop (Figure 1 a). Upon pinning of the drop, fingering instabilities set in owing to unfavorable interfacial interaction between the PS block and the Si substrate (PS possesses a positive value of the Hamaker constant A),^[19,20] thus resulting in the formation of a “coffee ring” with a serpentine appearance in the outer region of X (i.e., X_1 , where X is the distance from the sphere/Si contact center, Figure 1 b). The drop then depinned and formed a new ring with fingers, contracting the drop interface inward (Figure 2 a, taken in the intermediate region X_2). Finally, the drop reached the sphere/Si contact center (the inner region X_3) and the solution evaporated, locking in the patterns. Consequently, the repetitive pinning and depinning (i.e., stick–slip motion) of the contact line, together with the concurrent fingering instabilities of the rings, produced a

[*] S. W. Hong, J. Wang, Prof. Z. Lin
Department of Materials Science and Engineering
Iowa State University, Ames, IA 50011 (USA)
Fax: (+1) 515-294-7202
E-mail: zqlin@iastate.edu

[**] We gratefully acknowledge support from the National Science Foundation (NSF CAREER Award, CBET-0844084) and Air Force Office of Scientific Research (FA9550-09-1-0388).

Supporting information for this article is available on the WWW under <http://dx.doi.org/10.1002/anie.200903553>.

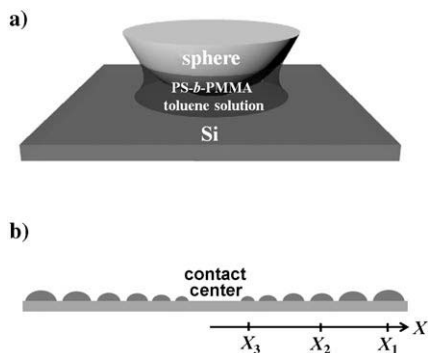


Figure 1. a) Schematic illustration of a drop of PS-*b*-PMMA diblock copolymer toluene solution constrained in a microscopic gap formed by placing a spherical lens in contact with a Si substrate (i.e., sphere-on-Si geometry), resulting in a capillary-held PS-*b*-PMMA solution. b) Cross section of concentric PS-*b*-PMMA coffee rings produced by controlled, repetitive pinning–depinning cycles of a three-phase contact line from the capillary edge as the solvent evaporates (Figure 1 a). The sphere/Si contact area is marked “contact center”. The distance of the rings from the contact center is X_n ($n=1-3$; X_1 , X_2 , and X_3 correspond to the outer, intermediate, and inner region, respectively, where the rings were formed).

lateral surface pattern consisting of hundreds of concentric, highly ordered serpentines with dimension gradient,^[21] as depicted in Figure 1 b and the left panel of Figure 2 b. AFM measurements of the serpentines deposited on the Si substrate revealed their dimensions and spacings. The characteristic wavelength of fingering instability along a serpentine λ_f , the average interserpentine distance λ_h , and the mean height of the serpentine h progressively decreased from $\lambda_f = 23.9 \mu\text{m}$, $\lambda_h = 17.9 \mu\text{m}$, and $h = 108.0 \text{ nm}$ at X_1 to $\lambda_f = 19.6 \mu\text{m}$, $\lambda_h = 16.2 \mu\text{m}$, and $h = 83.6 \text{ nm}$ at X_2 to $\lambda_f = 17.3 \mu\text{m}$, $\lambda_h = 10.5 \mu\text{m}$, and $h = 79.1 \text{ nm}$ at X_3 . A representative AFM image taken in the region X_2 is shown in Figure S1 in the Supporting Information; the ratio λ_f/λ_h was 1.21, and the height difference between two neighboring serpentines in close proximity Δt was 27.9 nm. Note that only a small zone of the concentric serpentines formed in the region X_2 is shown in Figure 2 a. The entire concentric serpentine pattern was produced over a surface area of $\pi\left(\frac{d}{2}\right)^2 = \pi\left(\frac{8}{2}\right)^2 \approx 50 \text{ mm}^2$, where d is the diameter of the outermost serpentine formed in the present study ($d = 8 \text{ mm}$). This area is dictated solely by the volume of the PS-*b*-PMMA solution and the diameter d (1 cm) of the spherical lens used. Using this technique, serpentines can be readily obtained over even larger areas by increasing d and applying a larger volume of polymer solution. The unique sphere-on-Si geometry provided an ideal environment for controlling flow within an evaporating droplet, which in turn resulted in well-ordered structure formation in one step.

The key to using block copolymers to produce hierarchically ordered materials lies in controlling the orientation of nanodomains.^[14,22] The preferential interaction of the PMMA block with the Si substrate, together with the lower surface energy of the PS block in cylinder-forming PS-*b*-PMMA diblock copolymer, forced the cylindrical PS nanodomains to orient themselves parallel to the surface. The surface tensions

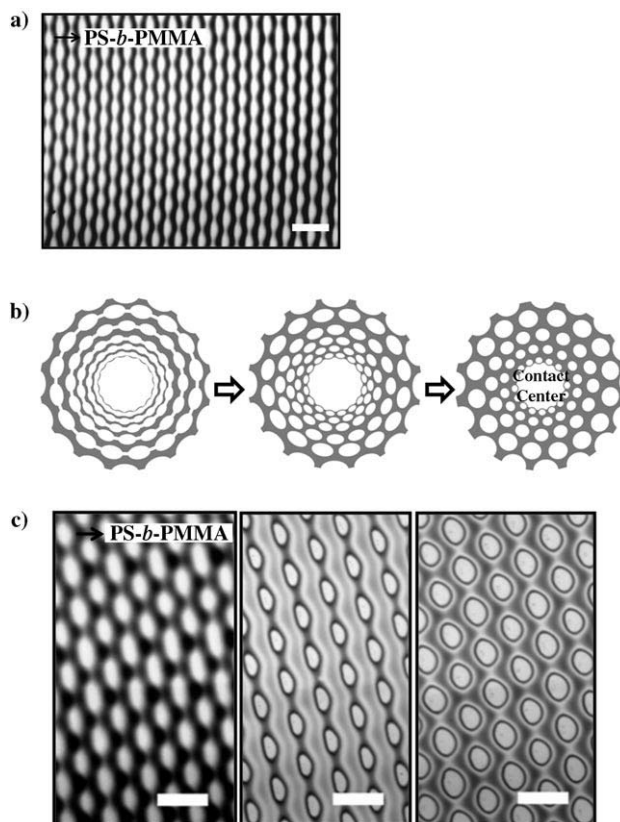


Figure 2. a) Optical micrograph of concentric serpentine PS-*b*-PMMA rings formed by repetitive stick–slip motion of the contact line in the sphere-on-Si geometry (Figure 1 a). Locally, these rings appear parallel to one another. Scale bar = 20 μm . b) Spatial–temporal evolution of concentric PS-*b*-PMMA serpentines into web-like macrostructures after lengthy solvent vapor annealing. c) Corresponding optical micrographs taken in situ during acetone vapor annealing. Left: As-prepared PS-*b*-PMMA serpentines before exposure to acetone vapor (0 h). Center: Selective swelling of PMMA blocks upon exposure to acetone vapor for 5 h; adjacent PS-*b*-PMMA serpentines interact with each other, forming periodic ellipsoidal holes. Right: Continuous acetone vapor annealing (12 h) leads to formation of regular microporous mesh arrays. Scale bars = 20 μm .

of PS and PMMA are $\gamma_{\text{PS}} = 40.7 \text{ mN m}^{-1}$ and $\gamma_{\text{PMMA}} = 41.1 \text{ mN m}^{-1}$, respectively.^[23,24] As a result, a disordered, nearly featureless topology of PS-*b*-PMMA was revealed by AFM measurement (lower left panel, Figure 3; taken in the intermediate region X_2). To achieve hexagonally packed arrays of nanoscopic PS cylinders oriented normal to the film surface in PS-*b*-PMMA, which would be more relevant technologically,^[13] selective solvent vapor annealing in a closed vessel for an appropriate time^[25,26] was undertaken after formation of the concentric serpentines (see the Experimental Section). Acetone is a strongly selective solvent for the PMMA block, the polymer–solvent interaction parameter of which ($\chi_{\text{PMMA/acetone}} = 0.18$) is less than $\chi_{\text{PS/acetone}}$ (1.1).^[25–27] The saturated solvent vapor annealing process effectively enhanced chain mobility in the diblock copolymers. The solvent vapor acts as a plasticizer and markedly lowers the glass transition temperature. The PMMA matrix was thus swollen by continuous absorption of acetone and

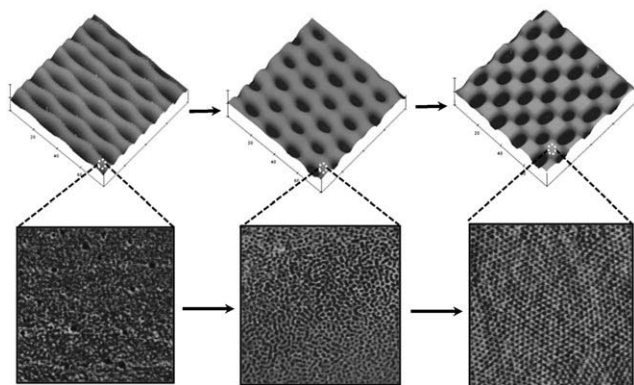


Figure 3. Evolution of regular PS-*b*-PMMA serpentine structures to hierarchically woven mesh arrays by acetone vapor annealing. Upper panels: AFM height images, corresponding to optical micrographs shown in Figure 2c: 0 (left), 5 (center), and 12 h (right). Scan size = $80 \times 80 \mu\text{m}^2$. Lower panels: Close-up AFM phase images from the surface of PS-*b*-PMMA patterns at each solvent annealing stage shown in the upper panels. Scan size = $2 \times 2 \mu\text{m}^2$. The originally disordered, almost featureless surface topology (left) transforms into well-ordered PS nanocylinders, which appear dark in the phase image and bright in the height image (Supporting Information, Figure S4). These nanocylinders are oriented vertically to the film surface (right) over the entire area of regular arrays.

pulled from the PMMA/Si interface to contact preferentially with the acetone vapor. The microphase separation of PS-*b*-PMMA diblock copolymer (i.e., the formation of disordered interconnected PMMA blocks at the film surface) is clearly evident after a short period of acetone vapor annealing (5 h; Figure 3, lower center, taken in the intermediate region X_2). Meanwhile, during annealing under the acetone vapor, the concentric serpentine rings of PS-*b*-PMMA deformed at the microscopic scale. Fingering instabilities on each serpentine amplified and interconnected with one another, forming periodic ellipsoidal holes. These are illustrated schematically in the central panel of Figure 2b as well as in a representative optical micrograph in the central panel of Figure 2c and an AFM image in the upper central panel of Figure 3. The λ_h is $16.7 \mu\text{m}$ and λ_f is $20.7 \mu\text{m}$ (Supporting Information, Figure S2); the ratio λ_f/λ_h is 1.24. The average height of the pattern was 83.6 nm , with a height difference between two adjacent holes Δt of 16.4 nm (Supporting Information, Figure S2).

These elliptical holes were further transformed into nearly circular holes upon longer solvent vapor treatment (12 h annealing; Figure 2b, right; Figure 2c, right; and Figure 3, upper right, taken in the intermediate region X_2), yielding $\lambda_h = 18.5 \mu\text{m}$ and $\lambda_f = 20.2 \mu\text{m}$, with the ratio $\lambda_f/\lambda_h = 1.09$ (Supporting Information, Figure S3). The average height of microstructures increased to 95.8 nm with no observable difference in height between two neighboring holes (Supporting Information, Figure S3), as was previously the case both before and after annealing for 5 h (Supporting Information, Figures S1 and S2). During this process, PS nanodomains self-assembled vertically to the entire PS-*b*-PMMA block copolymer surface, as revealed by AFM measurement (Figure 3, lower right; Supporting Information, Figures S4 and S5). The

characteristic distance between well-aligned PS nanocylinders λ_{C-C} was 66.5 nm ; the diameter of PS nanocylinders D was 38.6 nm . Hierarchically ordered arrays were thereby produced; close-packed, hexagonal PS nanocylinders were situated perpendicularly in regularly arranged local microscopic porous mesh structures within a global web of PS-*b*-PMMA, thus exhibiting self-assembly over length scales of several orders of magnitude. The evolution of polymer patterns from concentric serpentine rings to hierarchically ordered, macroscopic web-like patterns was monitored in situ by optical microscopy (see time-lapse video, Supporting Information, Movie S1). The ability to harness fingering instabilities in the serpentine PS-*b*-PMMA coffee rings is remarkable and may open avenues to study the fundamental fluid dynamics of the process, as well as to capitalize on the resulting patterns for potential uses in photonics, electronics, and microfluidic devices, among other applications.

Figure 4a illustrates the morphological reconstruction of PS-*b*-PMMA diblock copolymer from a nearly featureless topology to vertically oriented PS nanocylinders as a function of solvent vapor annealing time. Such structural rearrange-

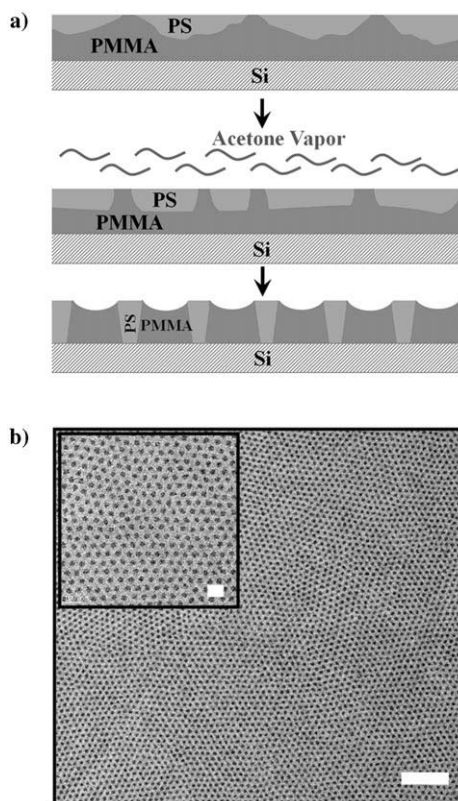


Figure 4. a) Schematic representation of formation of vertically aligned PS nanocylinders in the PMMA matrix as a function of solvent vapor annealing (side view). Owing to preferential interaction between the PMMA block and acetone, solvent vapor annealing imparts PMMA chain mobility, thereby transitioning the disordered, nearly featureless surface morphology (first panel) into PS nanocylinders that are vertical to the surface (last panel). b) TEM image of the bottom of the web-like PS-*b*-PMMA thin film formed after acetone vapor annealing for 12 h. The hexagonally ordered arrays of PS nanodomains appear dark in the bright PMMA matrix. Scale bars are 500 and 100 nm in the main image and the inset, respectively.

ment was primarily due to the migration of the PMMA matrix, which interacted preferentially with acetone vapor. Surface reconstruction processes in thin block copolymer films have been an area of intense research.^[17,28,29] As PS and PMMA blocks are covalently linked at one end, the PS domains rearranged themselves accordingly, thereby leading to microphase-separated morphologies (Figure 3, center and right). To verify this reconstruction mechanism, the surface composition of the PS-*b*-PMMA patterns formed at different annealing times (0, 5, and 12 h) were examined using X-ray photoelectron spectroscopy (XPS), as summarized in Figure S6 in the Supporting Information. For the unannealed sample (0 h), the hydrocarbon peak (C–C and C–H) at a binding energy of 285.0 eV and the weak carbonyl peak at 289.1 eV (O–C=O) from the PMMA matrix were present, suggesting that both PS and PMMA blocks existed at the surface. The PS blocks segregated preferentially (but not exclusively) to the air interface, in agreement with the AFM measurement in the lower left panel of Figure 3. The carbonyl peak gradually increased in intensity with increased exposure time, signifying that the PMMA matrix was in contact with the air surface. To confirm the vertical orientation of the PS nanodomains from the air surface to the substrate across the entire web-like macrostructures after 12 h annealing, transmission electron microscopy (TEM) imaging was performed by examining the bottom of the resulting patterns originally in contact with the substrate (see the Experimental Section). The hexagonally ordered arrays of PS nanodomains that appeared dark in the bright PMMA matrix were observed in all regions (X_1 , X_2 , and X_3); a typical TEM image taken in the intermediate region X_2 is shown in Figure 4b. This morphology is identical to that on the top of the web captured by AFM (Figure 3, lower right; Supporting Information, Figure S4). The characteristic distance between adjacent PS nanodomains λ_{C-C} and the diameter of PS nanodomains D were 64.6 and 31.6 nm, respectively (inset, Figure 4b). It is clear that λ_{C-C} remained nearly constant at both the top and bottom of the web, while D on the bottom surface (Figure 4b) was slightly smaller than on the top surface measured by AFM (Figure 3, lower right). This observation suggests that a slightly larger amount of PMMA matrix may be present on the Si substrate owing to the strong affinity of PMMA with a thin native layer of silicon oxide on the Si substrate.

It is worth noting that, as opposed to thermally equilibrated block copolymer thin film morphologies, hierarchically ordered structures produced by the solvent vapor annealing process are far from equilibrium. In these structures, the PS nanodomains are higher than the PMMA matrix (last panel, Figure 4a; Supporting Information, Figure S4a), and in AFM phase images they appear dark compared to the PMMA matrix (Figure 3, lower right; Supporting Information, Figure S4b). This effect is due to selective swelling of the PMMA matrix by acetone vapor and subsequent contraction upon the evaporation of acetone.^[24,25] Notably, these intriguing, functional polymeric macrostructures with hierarchical order are highly reproducible. If the PMMA matrix were selectively removed, the macrostructures would have PS nanopillars, which can be utilized as a template to produce a wide range of nanoporous metallic or metal oxide films.^[30,31]

We present a simple, scalable, low-cost, lithography-free method for creating nanostructured materials that exhibit unique and highly regular structural hierarchies over large areas. The method is based on the controlled evaporative self-assembly of block copolymers in a sphere-on-Si geometry with subsequent solvent vapor annealing. The resulting multiscale hierarchical structures should enable the spatially defined incorporation of nanocrystals such as quantum dots and ferroelectric nanoparticles to yield hierarchically ordered multifunctional materials. These structures may find potential applications in optical, electronic, and photonic devices;^[32] magnetic materials;^[13] nanotechnology;^[13] and biotechnology.^[33] Furthermore, these structures may also serve as platforms to study cell adhesion and motility, neuron guidance, and cell mechanotransduction.^[34] By the judicious choice of shapes other than spheres for the upper surface,^[35] we anticipate the creation of a rich family of complex, hierarchically assembled surface patterns of varying architectures formed by the synergy of the stick-slip motion and controlled fingering instabilities at the microscopic scale but also influenced by the self-assembly of block copolymers with different morphologies (spheres, cylinders, or lamellae) and chemical structures (glassy, semicrystalline, or rubbery blocks) at the nanoscale.

Experimental Section

Evaporative self-assembly of diblock copolymer at the micrometer scale: An asymmetric diblock copolymer, polystyrene-*b*-poly(methyl methacrylate) (PS-*b*-PMMA; number average molecular weight: PS 45.9 kg mol⁻¹, PMMA 138 kg mol⁻¹; polydispersity 1.16; Polymer Source, Inc.) was dissolved in toluene at a concentration of 0.13 mg mL⁻¹ and purified with 200 nm polytetrafluoroethylene (PTFE) filters. The silicon substrate and spherical lens made from fused silica (radius of curvature 1.65 cm, diameter 1 cm) were cleaned with a mixture of sulfuric acid and Nochromix. They were then rinsed extensively with deionized (DI) water and blow-dried with filtered N₂. A sphere-on-Si geometry was implemented as follows. The spherical lens and Si substrate were firmly fixed at the top and bottom of sample holders, respectively. An inchworm motor was used to bring the upper sphere nearly into contact with the lower stationary Si substrate. Before contact, with just a few hundred micrometers between the two surfaces, PS-*b*-PMMA toluene solution (15 μ L) was loaded and confined between the sphere and the Si substrate by capillary forces. The sphere was finally moved into contact with the Si substrate so that a capillary-held polymer solution resulted, with the evaporation rate highest at the extremity, as schematically illustrated in Figure 1a. The evaporation took approximately 30 min to complete. Afterward, the sphere and the Si substrate were separated, and the patterns on the substrate were examined.

Self-assembly of diblock copolymer at the nanoscale induced by solvent vapor annealing: The regular PS-*b*-PMMA patterns formed on the Si substrate were exposed to acetone vapor for a certain period of time in a closed vessel to achieve microphase separation of PS-*b*-PMMA. The 33 cm³ vessel was filled with 3.5 mL acetone. The vessel was placed in an aluminum chamber to avoid temperature variation.

TEM sample preparation: A drop of DI water was placed on a web-like film formed on the mica surface; the film then spontaneously delaminated from the mica surface and floated on the surface of the water. A TEM grid was then placed in contact with the top of the floated film, thereby exposing the bottom of the film on the TEM grid surface. Finally, the grid was exposed to ruthenium tetroxide (RuO₄), with which the PS phase was preferentially stained. As a

result, PS nanodomains appeared dark in TEM images (JEOL 2100 Scanning and Transmission Electron Microscope (STEM) at the Microscopy and Nanoimaging Facility (MNIF) of Iowa State University, operating at 200 kv).

Characterization: To examine the morphology of regular PS-*b*-PMMA block copolymer patterns formed on the Si substrate, optical microscopy (OM; Olympus BX51) measurements in the reflection mode and atomic force microscopy (AFM; Digital instruments Dimension 3100 scanning force microscope) imaging in the tapping mode were performed. Only the morphologies formed in the intermediate region X_2 imaged by OM and AFM were presented. Confirmation of migration of the PMMA block to the surface was obtained by X-ray photoelectron spectroscopy (XPS; Perkin-Elmer $Al_{K\alpha}$ X-ray source, 250 W).

Received: June 30, 2009

Revised: August 3, 2009

Published online: September 24, 2009

Keywords: block copolymers · hierarchically ordered structures · self-assembly · surface patterning

-
- [1] R. D. Deegan, O. Bakajin, T. F. Dupont, G. Huber, S. R. Nagel, T. A. Witten, *Nature* **1997**, 389, 827.
- [2] E. Adachi, A. S. Dimitrov, K. Nagayama, *Langmuir* **1995**, 11, 1057.
- [3] E. Pauliac-Vaujour, A. Stannard, C. P. Martin, M. O. Blunt, I. Nottingher, P. J. Moriarty, I. Vancea, U. Thiele, *Phys. Rev. Lett.* **2008**, 100, 176102.
- [4] V. X. Nguyen, K. J. Stebe, *Phys. Rev. Lett.* **2002**, 88, 164501.
- [5] E. Rabani, D. R. Reichman, P. L. Geissler, L. E. Brus, *Nature* **2003**, 426, 271.
- [6] M. Gleiche, L. F. Chi, H. Fuchs, *Nature* **2000**, 403, 173.
- [7] J. Huang, F. Kim, A. R. Tao, S. Connor, P. D. Yang, *Nat. Mater.* **2005**, 4, 896.
- [8] D. J. Harris, H. Hu, J. C. Conrad, J. A. Lewis, *Phys. Rev. Lett.* **2007**, 98, 148301.
- [9] H. Yabu, M. Shimomura, *Adv. Funct. Mater.* **2005**, 15, 575.
- [10] T. P. Bigioni, X. M. Lin, T. T. Nguyen, E. I. Corwin, T. A. Witten, H. M. Jaeger, *Nat. Mater.* **2006**, 5, 265.
- [11] B. Pokroy, S. H. Kang, L. Mahadevan, J. Aizenberg, *Science* **2009**, 323, 237.
- [12] B. P. Khanal, E. R. Zubarev, *Angew. Chem.* **2007**, 119, 2245; *Angew. Chem. Int. Ed.* **2007**, 46, 2195.
- [13] T. Thurn-Albrecht, J. Schotter, C. A. Kastle, N. Emley, T. Shibauchi, L. Krusin-Elbaum, K. Guarini, B. C. T. , M. T. Tuominen, T. P. Russell, *Science* **2000**, 290, 2126.
- [14] C. J. Hawker, T. P. Russell, *MRS Bull.* **2005**, 30, 952.
- [15] J. Y. Cheng, C. A. Ross, H. I. Smith, E. L. Thomas, *Adv. Mater.* **2006**, 18, 2505.
- [16] S. Ouk Kim, H. H. Solak, M. P. Stoykovich, N. J. Ferrier, J. J. de Pablo, P. F. Nealey, *Nature* **2003**, 424, 411.
- [17] S. Park, D. H. Lee, J. Xu, B. Kim, S. W. Hong, U. Jeong, T. Xu, T. P. Russell, *Science* **2009**, 323, 1030.
- [18] C. Tang, E. M. Lennon, G. H. Fredrickson, E. J. Kramer, C. J. Hawker, *Science* **2008**, 322, 429.
- [19] P. Lambooy, K. C. Phelan, O. Haug, G. Krausch, *Phys. Rev. Lett.* **1996**, 76, 1110.
- [20] M. D. Morariu, E. Schaffer, U. Steiner, *Eur. Phys. J.* **2003**, 12, 375.
- [21] J. Xu, J. Xia, S. W. Hong, Z. Q. Lin, F. Qiu, Y. L. Yang, *Phys. Rev. Lett.* **2006**, 96, 066104.
- [22] R. A. Segalman, *Mater. Sci. Eng. R* **2005**, 48, 191.
- [23] S. Wu, *J. Phys. Chem.* **1970**, 74, 632.
- [24] M. Byun, S. W. Hong, F. Qiu, Q. Zou, Z. Lin, *Macromolecules* **2008**, 41, 9312.
- [25] Y. Xuan, J. Peng, L. Cui, H. Wang, B. Li, Y. Han, *Macromolecules* **2004**, 37, 7301.
- [26] J. Peng, D. H. Kim, W. Knoll, Y. Xuan, B. Li, Y. Han, *J. Chem. Phys.* **2006**, 125, 064702.
- [27] Y. Chen, H. Huang, Z. Hu, T. He, *Langmuir* **2004**, 20, 3805.
- [28] T. Xu, J. Stevens, J. A. Villa, J. T. Goldbach, K. W. Guarini, C. T. Black, C. J. Hawker, T. P. Russell, *Adv. Funct. Mater.* **2003**, 13, 698.
- [29] S. Park, B. Kim, J. Xu, T. Hofmann, B. M. Ocko, T. P. Russell, *Macromolecules* **2009**, 42, 1278.
- [30] K. Shin, K. A. Leach, J. T. Goldbach, D. H. Kim, J. Y. Jho, M. Tuominen, C. J. Hawker, T. P. Russell, *Nano Lett.* **2002**, 2, 933.
- [31] Y. Gong, W. Joo, Y. Kim, J. K. Kim, *Chem. Mater.* **2008**, 20, 1203.
- [32] H. O. Jacobs, G. M. Whitesides, *Science* **2001**, 291, 1763.
- [33] E. Delamarche, A. Bernard, H. Schmid, B. Michel, H. Biebuyck, *Science* **1997**, 276, 779.
- [34] X. Chen, M. Hirtz, H. Fuchs, L. Chi, *Langmuir* **2007**, 23, 2280.
- [35] S. W. Hong, M. Byun, Z. Q. Lin, *Angew. Chem.* **2009**, 121, 520; *Angew. Chem. Int. Ed.* **2009**, 48, 512.
-